Adsorption (2015) 21:77–86
DOI 10.1007/s10450-015-9651-2

# Chromium-based metal–organic framework/mesoporous carbon composite: synthesis, characterization and $CO_2$ adsorption

**Zhongzheng Zhang · Hui Wang · Xinqing Chen · Chenming Zhu · Wei Wei · Yuhan Sun**

Received: 21 August 2014 / Revised: 4 January 2015 / Accepted: 12 January 2015 / Published online: 29 January 2015


**Abstract** New composites of a water-stable chromium-based metal organic framework MIL-101 and mesoporous carbon CMK-3 were in situ synthesized with different ratios of MIL-101 and CMK-3 using the hydrothermal method. The composites as well as the parent materials were characterized by X-ray diffraction, thermo gravimetric analysis, scanning electron microscope, transmission electron microscope and nitrogen/carbon dioxide adsorption isotherms. The hybrid material possesses the same crystal structure and morphology as its parent MIL-101, and exhibits an enhancement in $CO_2$ adsorption uptakes when compared to MIL-101 and CMK-3. The increase in $CO_2$ uptakes was attributed to the combined effect of the formation of additional micropores, the enhancement of micropore volume and the activation of unsaturated metal sites by CMK-3 incorporation.

**Keywords** MOFs · CMK-3 · $CO_2$ adsorption · MOFs composites · MIL-101

## 1 Introduction

Carbon dioxide ($CO_2$), the most prevalent greenhouse gas mainly from the burning of fossil fuels, has been identified as the major contributor to global warming and climate change. Considering more than 80 % world's energy supply will continue to rely on fossil fuels in the next 20–30 years, the exploration of effective ways to reduce the release of $CO_2$ into the atmosphere is very important for the fossil fuel industrial society. Among different strategies proposed for $CO_2$ capture, $CO_2$ capture by adsorption in porous materials has been determined as one of the most potential ways considering the low cost of equipment and the possible recycling uses of the captured $CO_2$ (Wong and Bioletti 2002). Nevertheless, excellent adsorbent materials with high uptake capacity, high selectivity and mild regeneration condition are the prerequisite of successfully applying the method in $CO_2$ capture from flue gas.

Up to date, various porous solid adsorbents, such as zeolites (Shao et al. 2009; Miyamoto et al. 2012), activated carbons (Guo et al. 2006; Yang et al. 2011), metal oxides (Martacaltzi and Lemonidou 2008; Li et al. 2010), and mesoporous silica and carbon (Sun et al. 2007; Govindasamy et al. 2009), and their amine-modified materials (Chang et al. 2009; Li et al. 2013), has been developed as effective $CO_2$ capture adsorbents, but the common shortfalls of these traditional adsorbents are either low capacities and selectivity or difficult regeneration processes (Zhang et al. 2011, 2013).

Recently, metal–organic frameworks (MOFs) have been evaluated as promising $CO_2$ capture adsorbents due to their extremely high surface area, giant pore volume and tunable pore size. It has been reported that many MOFs have higher $CO_2$ uptakes than traditional adsorbents under both high pressures and atmospheric pressures (Millwar and Yaghi 2005; Liewellyn et al. 2008; Furukawa et al. 2010; Liu et al. 2010; Yazaydin et al. 2009). However, the porosity of MOFs is often not fully utilized during adsorption process

Z. Zhang · H. Wang · X. Chen · C. Zhu · W. Wei (✉)
Center for Greenhouse Gas and Environmental Engineering, Shanghai Advanced Research Institute, Chinese Academy of Sciences, Shanghai 201203, China
e-mail: weiwei@sari.ac.cn

Z. Zhang · H. Wang · X. Chen · C. Zhu · W. Wei · Y. Sun
CAS Key Laboratory of Low-Carbon Conversion Science and Engineering, Shanghai Advanced Research Institute, Chinese Academy of Science, Shanghai 201203, China

because of the weak interactions between the walls of MOFs and small gas molecules due to the low density of atoms in MOFs and fully open pore space (Suddik et al. 2006). Taking into account this drawback, one could hybrid MOFs with other porous materials to form MOF composites, which often result in new or modified properties than that of individual counterparts. The introduction of porous materials in the composites not only favors the dispersive forces and provides extra adsorptive sites (Petit and Bandosz 2009, 2010), but also optimizes the pore diameter and creates additional porosity (Petit et al. 2011; Rallapalli et al. 2013), resulting in higher gas adsorption uptake than that of the parent materials.

Recently, a few studies on hybridizing MOF-5 with mesoporous silica SBA-15 (Wu et al. 2013), carbon nanotubes (Pachfule et al. 2012), carbon nanofibers (Yang et al. 2009) and graphite oxide (Petit and Bandosz 2009) have been reported. These hybrid materials exhibit improved hydrothermal stability and significant enhancements in gas adsorption capacities. Despite the encouraging results of the MOF-5 composites mentioned above, the collapse of MOF-5 structure in the humidity limits the further applications of the synthesized composites at ambient conditions (Kaye et al. 2007). Considering this weak point of MOF-5 composites as well as the promising concept of MOF composites, some researchers prepared new composites made of water-stable MOF components, such as MIL-101 (Petit and Bandosz 2010; Prasanth et al. 2011), HKUST-1 (Petit et al. 2011, 2010) and ZIF-8 (Kumar et al. 2013), with activated carbon or graphite oxide. Most of the literatures about MOF composites are focused on $H_2$ storage and $NH_3$ uptake. Recently, some reports about $CO_2$ capture and adsorption mechanism on HKUST-1 composites with graphite oxide or aminated graphite oxide have been extensively studied (Zhao et al. 2013, 2014; Policicchio et al. 2014), and all the results showed that $CO_2$ adsorption capacity on these MOF composites were enhanced significantly in comparison with their individual counterparts. To the best of our knowledge, there have been no published accounts of MOF composite materials composed of an ordered mesoporous carbon phase.

Therefore, the objective of this study is to prepare and characterize an ordered mesoporous carbon–metal organic composite material. In this paper, chroumium-based MOF MIL-101 and mesoporous carbon CMK-3 were selected and MIL-101/CMK-3 (referred to as MC) composites with different amounts of CMK-3 were synthesized through in situ hydrothermal method. Characterization methods for the composites include $N_2$ adsorption isotherms, X-ray diffraction (XRD), element analysis, thermogravimetric analysis, scanning electron microscopy (SEM), transmission electron microscopy (TEM) and $CO_2$ adsorption.

## 2 Experimental

### 2.1 Raw materials

Triblock copolymer $EO_{20}PO_{70}EO_{20}$ (P123, Aldrich, M.w. 5800,), Tetraethyl orthosilicate (TEOS, Sinopharm Chemical Reagent, China, AR), Terephthalic acid ($H_2BDC$, Shanghai Richjoint Chemical Reagents, China, 99 %), chromium nitrate ($Cr(NO_3)_3.9H_2O$, Shanghai Richjoint Chemical Reagents, 99 %), hydrofluoric acid (HF, Shanghai Shenbo Chemical, China, 40 %), dimethylformamild (DMF, Chinasun Specialty Products, China, 99.5 %) and ammonium fluoride ($NH_4F$, Chinasun Specialty Products, China, 96 %) were all used without any further purification.

All the gases used in the adsorption measurements were highly purified (99.995 %).

### 2.2 Synthesis of CMK-3

The synthesis of CMK-3 was made using SBA-15 silica as the template and sucrose as the carbon source. High-quality SBA-15 sample was prepared using the surfactant P123 and the silica source TEOS following the procedure reported by Zhao (Zhao et al. 1998). Typically, 12.5 g of TEOS was added dropwise into 240 mL of 1 M HCl containing 6 g of P123 at 308 K. The mixture was stirred for 24 h at 308 K, and then transferred into Teflon-lined stainless steel autoclave and aged for another 24 h at 393 K. The product was filtered, washed with ethanol, dried and subsequently calcined at 823 K for 6 h.

The calcined SBA-15 was impregnated with aqueous solution of sucrose and sulfuric acid according to the literature (Jun et al. 2000): 1 g of SBA-15 was added to a solution of 1.25 g of sucrose and 0.14 g of $H_2SO_4$ in 5 g of water. The mixture was placed for 6 h at 373 K, and then for another 6 h at 423 K. The obtained dark brown sample, containing partially polymerized and carbonized sucrose, was treated again at 373 and 423 K after the addition of 0.8 g of sucrose, 0.09 g of $H_2SO_4$ and 5 g of $H_2O$. The carbonization was completed by pyrolysis at 1173 K under N2 flow for 6 h, and the carbon–silica composite was treated with 1 M NaOH solution twice at 373 K to remove the silica template. At last, the template-free carbon product CMK-3 was filtered, washed with water, and dried at 393 K.

### 2.3 Synthesis of MIL-101

A typical synthesis process was performed following the reported procedure (Férey et al. 2005). The mixture of $Cr(NO_3)_3.9H_2O$ (4.00 g), deionized water (48 $cm^3$), $H_2BDC$ (1.64 g) and HF (0.50 $cm^3$) was sonicated at room

temperature for 20 min, and then transferred into a Teflon-lined autoclave for 8 h at 493 K. After cooling to ambient temperature, a fine green-colored powder was obtained as the major product and significant amounts of non-reacted $H_2BDC$ were still present in the form of needle-shaped colorless crystals along with the product.

The unreacted $H_2BDC$ was removed by three-stage solvent extraction. The crude product was treated with 150 mL of DMF under stirring for 1 h, which was repeated for twice. Then, the DMF-treated product was activated by 150 mL of ethanol at 373 K for 20 h, and subsequently by 150 mL of 0.03 M $NH_4F$ aqueous solution at 333 K for 10 h. Finally, the purified product MIL-101 was filtered, washed with hot water to remove trances of $NH_4F$, and dried at 423 K for 24 h under vacuum.

### 2.4 Synthesis of MC composite

The in situ synthesis of MC composite was similar to the preparation of MIL-101, and the purification process was also performed under the same conditions as MIL-101. The difference was that CMK-3 was added simultaneously along with the raw materials during the synthesis of MC composite. The amount of CMK-3 was varied from 30 to 60 mg to prepare different samples of MC composites, and they were denoted as MC-30 and MC-60, respectively.

After complete activation, the obtained final weight of sample MIL-101, MC-30 and MC-60 was 1.208, 1.289 and 1.367 g, respectively. Since CMK-3 phase was incorporated into the framework of MIL-101 crystals (discussed later), it was supposed that there was no weight loss of CMK-3 in the synthesis and activation processes for MC-30 and MC-60 sample. Thus, the loading contents of CMK-3 in the MC-30 and MC-60 sample could be estimated to be 2.3 wt% and 4.4 wt%, respectively.

### 2.5 Characterization

XRD patterns of the samples before and after CMK-3 incorporation were obtained at ambient temperature on a Rigaku D/MAX IIIB diffractometer with Cu-butt at the conditions of 40 kV and 30 mA. The scan range was from 5° to 20° at 2°/min with a step size of 0.05° and step time 1 s.

The thermal stability of MIL-101 and CMK-3-incorporated MIL-101 samples were investigated using a thermogravimetric analyzer (TGA, Mettler Toledo 851) in a flowing $N_2$ atmosphere (40 $cm^3$/min) from 25 to 800 °C with a heating rate of 10 K/min.

The elemental composition of the samples was accomplished by CHN analyzer Perkin Elmer-2400. SEM was performed on JEOLJSM-6380LV instrument. TEM was performed on a JEOL 2100F instrument.

The textural properties of MIL-101 and its composite materials were determined from $N_2$ adsorption isotherms collected at 77 K with instrument ASAP 2020. The specific surface area and pore size distribution (PSD) were evaluated with the BET and BJH method, and the total pore volume was calculated on the basis of the $N_2$ adsorption amounts at $p/p^0 = 0.99$. Prior to adsorption measurements, the samples were degassed for 24 h at 423 K under vacuum to remove any guest molecules from the pores.

High-pressure gas adsorption measurements from 0 to 5 Mpa were carried out on a homemade volumetric adsorption apparatus. The relative precision of used pressure transducer was 0.01 % for the range of 20 MPa. Temperature was kept constant within ±0.01 °C. Helium was used to calibrate dead volume and volume of sample cell with sample. Before adsorption measurements, the sample was activated in a vacuum at 423 K for 24 h.

## 3 Results and discussion

The XRD patterns of MIL-101 and MC composites are shown in Fig. 1. The XRD pattern of MIL-101 in Fig. 1a is in accordance with the literature data (Krungleviciute et al. 2007). This proves the successful synthesis procedure. The XRD patterns of the MC composites are similar to that of its parent MIL-101, which indicates the existence of the MIL-101 units in the synthesized materials. Thus, we could assume that the addition of porous material CMK-3 does not affect the structure of MIL-101. On the other hand, it is interesting to note that the characteristic peak of CMK-3 around 2Theta 0.99° is not found in the composites' small angle diffraction patterns. One reason is that the loading content of CMK-3 is very low, and another more important reason is that CMK-3 material was embedded inside the crystal framework, which is ca. 500 nm indicated from Fig. 3b, c, which may be attributed to the nucleating effect of CMK-3 in the formation of MIL-101 microcrystals. The same experimental finding was also observed in the literature (Buso et al. 2011), in which D. Buso have successfully incorporated $SiO_2$ nanoparticles into MOF-5 frameworks although the average diameters of $SiO_2$ (153 nm) was much far larger than MOF-5 pore size.

In addition, the addition of porous material CMK-3 in the synthesis process of MIL-101 does not weaken the thermal stability of MC composites when compared to parent MIL-101, shown by TGA plots in Fig. 2.

Figure 3a–c show the SEM images of MIL-101 and MC composites. The cubic symmetry of MIL-101 is reflected in the shape of the crystals. Little amount of incorporated CMK-3 does not disrupt the morphology of MC-30 while there was a change in the surface morphology of MC-60 when extra carbon was added. The TEM image of MC-60

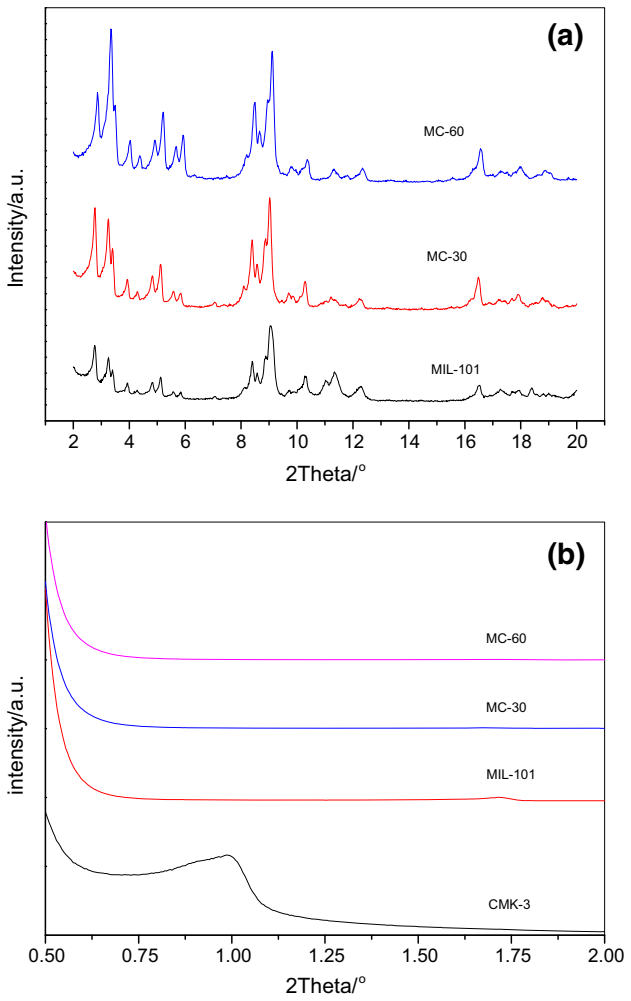


**Fig. 1** XRD patterns of MIL-101, CMK-3 and MC composites. **a** wide angle XRD; **b** small angle XRD

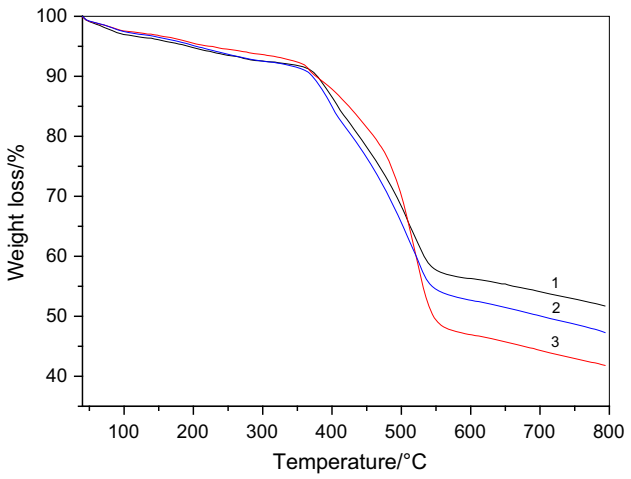


**Fig. 2** TGA plots of MIL-101 and MC composites *1* MIL-101; *2* MC-30; *3* MC-60

shown in Fig. 3d reveals that CMK-3 was indeed well incorporated into MIL-101 crystallites and the hybrid composite, especially in the selected red region, shows two distinctive pore spacing of about 3.6 nm which is in consistent with pore size of CMK-3.

Since both HKUST-1 and MIL-101 contains unsaturated metal sites, the MC composite formation mechanism is supposed to be similar to that of HKUST-1/grapheme oxide composite (Petit et al. 2011; Zhao et al. 2014). During the synthesis of the MC composite, bigger carbon particles were broken up into smaller particles under ultra-sonication. It is the smaller size of carbon particles as well as the presence of a number of functional groups including hydroxyl and carboxyl on the surface and pore channels of CMK-3 after treatment with 3 M $HNO_3$ for 6 h at 50 °C that makes CMK-3 carbon phase more easily encapsulated in the MIL-101 framework via the reaction between the Cr(III) unsaturated sites of MIL-101 and the functional groups on CMK-3 surface. The reactions of the carboxylic groups with the Cr(III) sites of MIL-101 can be expected since the H2BDC organic ligand already presents such functionalities. Regarding the hydroxylic groups, their interactions with the chromium sites can be compared to interactions with water.

$N_2$ adsorption–desorption isotherms at 77 K in MC composites as well as its individual counterparts are depicted in Fig. 4. The isotherm obtained for CMK-3 is of typical Type-IV characteristic for mesoporous materials, while the isotherms for MIL-101 and its composites are of Type-I where there are secondary uptakes near 0.1 and 0.2 of relative pressure which are caused by two kinds of microporous windows reported by Férey (Férey et al. 2005). However, there are no any features of CMK-3 isotherm in MC composites, such as capillary condensation phenomenon and hysteresis loop. This may be due to two reasons, the low content of CMK-3 carbon phase and the embedding of CMK-3 in the MOF framework, which has been confirmed by the TEM image of MC-60 composite shown in Fig. 3d. Besides, another possible reason was that the mesopore channels of CMK-3 was likely occupied by inorganic chromium-trimers and/or super-tetrahedron building units formed by organic ligands and trimeric chromium octahedral clusters.

Table 1 lists the textural properties of MIL-101, CMK-3 and CMK-3-embedded composites, as determined from $N_2$ isotherms at 77 K. The BET surface area for MIL-101 is as high as 4824 $m^2/g$, which is even larger than the highest values reported in other papers (Liu et al. 2007; Maksimchuk et al. 2008; Liu et al. 2012). This proves that the purification steps are successful in removing all unreacted $H_2BDC$ impurities presented in MIL-101 pores, which is also indicated by SEM image of MIL-101 in

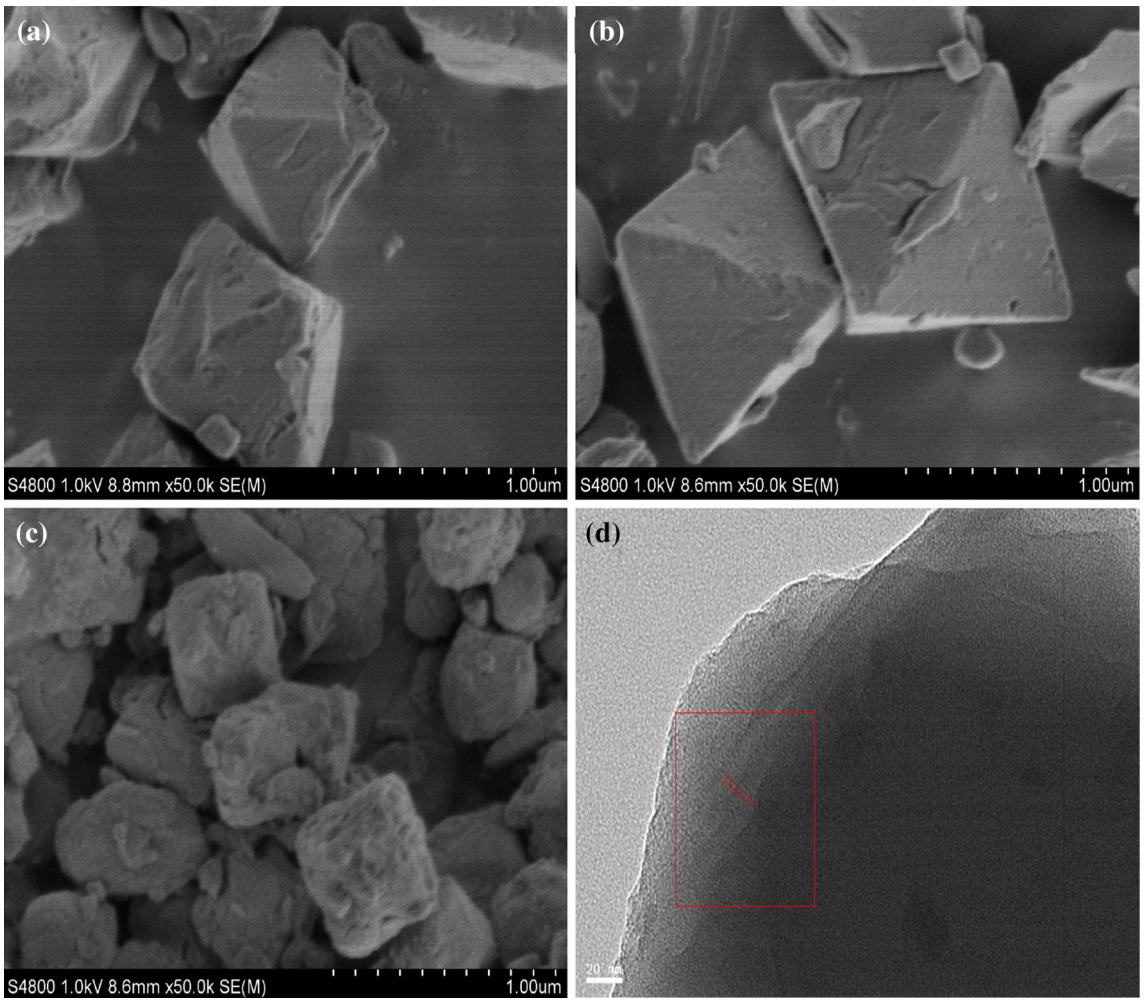


**Fig. 3** SEM images of **a** MIL-101, **b** MC-30, **c** MC-60 and TEM image of **d** MC-60

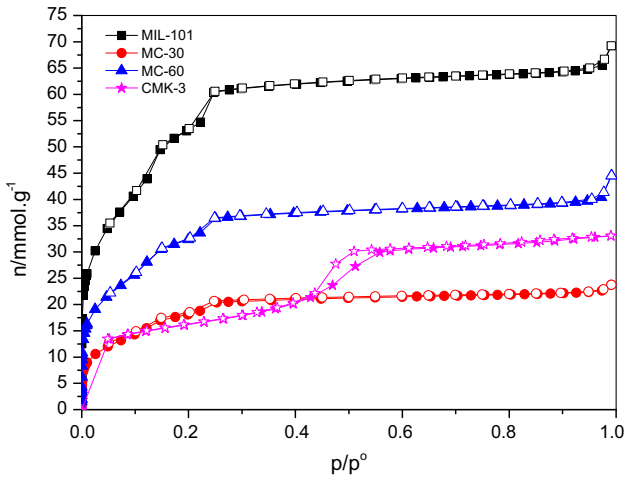


**Fig. 4** $N_2$ adsorption–desorption isotherms in MIL-101, CMK-3 and MC composites

Fig. 3 since no traces of $H_2BDC$ are observed in MIL-101 crystals. However, MC composites' BET surface area is much lower than pure MIL-101. In addition, there is more free space in an "empty" MIL-101 than in the same MOF composites, which also suggests that MIL-101 was partially filled with CMK-3 material. Besides, we can find that there are very small differences in carbon content of pure MOF and composites, which just indicates the added amount of CMK-3 in composites is very small.

PSD curves of MIL-101 and MC composites estimated by NLDFT method are shown in Fig. 5, as well as the PSD curve of CMK-3 calculated by BJH method. There are four maxima centered at pore radii of ca. 1.3, 1.8, 2.6 and 3.5 nm for MIL-101 material, which match well with the theoretical pore size of pentagonal window, hexagonal window, middle cage and large cage of the crystal structure of MIL-101. The incorporation of CMK-3 into MIL-101 framework didn't change the pore diameter for MC composites. However, the characteristic pore size (3.8 nm) of CMK-3 was not observed in MC composites mainly due to the low content of CMK-3 in composites and the possible occupation of meso-channels by some Cr-containing phases.

**Table 1** Textural properties of MIL-101, CMK-3 and MC composites

| Sample | Carbon content[a]/% | BET surface area/$m^2$ $g^{-1}$ | Pore volume/$cm^3$ $g^{-1}$ | Pore volume of micropores/$cm^3$ $g^{-1}$ |
|---|---|---|---|---|
| MIL-101 | 35.31 | 4824 | 2.41 | 1.55 |
| MC-30 | 36.80 | 1586 | 0.83 | 0.36 |
| MC-60 | 38.97 | 2828 | 1.55 | 0.67 |
| CMK-3 | – | 1223 | 1.15 | 0 |

[a] Determined by CHN analyzer, thus the value attributed to the carbon from both CMK-3 and MIL-101

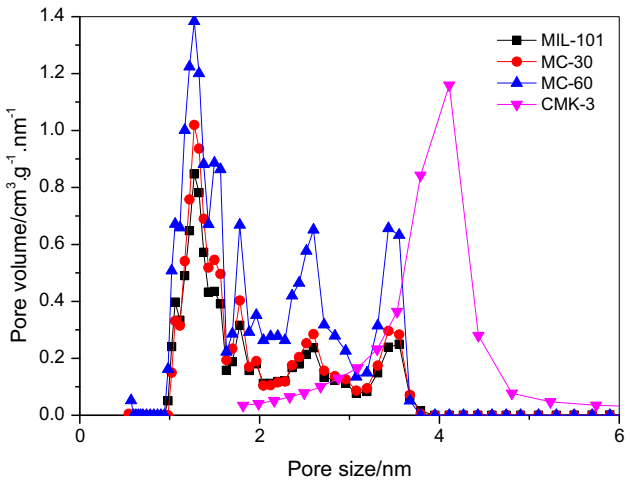


**Fig. 5** Pore size distribution of MIL-101, CMK-3 and MC composites

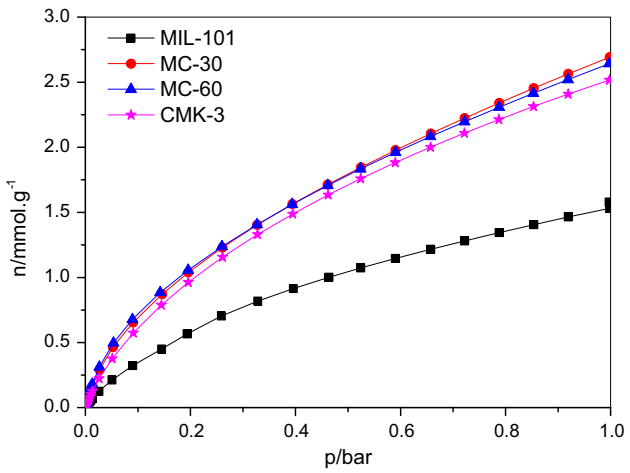


**Fig. 6** $CO_2$ adsorption isotherms at 298 K

In order to examine $CO_2$ capture performance of MC composites, $CO_2$ adsorption at 298 K up to 1 bar was performed and shown in Fig. 6. The $CO_2$ uptake for MIL-101 exhibits 1.52 mmol/g at 1 atm. The value of $CO_2$ uptake on MIL-101 is lower than that obtained by Llewellyn (Liewellyn et al. 2008) although the surface area and total pore volume of the as-synthesized MIL-101 in this paper are larger than that made by Llewellyn. This suggests that surface area and total pore volume are not the crucial factors influencing $CO_2$ uptake at low pressure. Liu (Liu et al. 2012) reported that keys to $CO_2$ adsorption at low pressures in MOF are summarized to be heats of adsorption, which was related to, as we known, active adsorption sites. Therefore, the adsorption enthalpy of $CO_2$ on our MIL-101 sample was calculated with the Clausius–Clapeyron equation (Arstad et al. 2008) based on two isotherms of $CO_2$ at 298 K (Fig. 9) and 308 K (Fig. 10). The plots of adsorption enthalpy as a function of $CO_2$ uptakes were shown in Fig. 7. As we can see, the value of adsorption enthalpy at the onset of adsorption was the same as the reported value by Llewellyn, but it decreases much faster with the increase in $CO_2$ loading than Llewellyn report. This indicates that in our MIL-101 sample there exist unsaturated metal sites (UMS), but the number of UMS was much low, which was likely the reason for the deference in $CO_2$ uptakes between our MIL-101 sample and Llewellyn's. From the comparison of $CO_2$ adsorption heat on MIL-101 and MC-60 composite (Fig. 7), we could find that the difference in the initial adsorption enthalpy is very small, which may be attributed to the preferred adsorption of $CO_2$ molecules on Cr(III) unsaturated metal

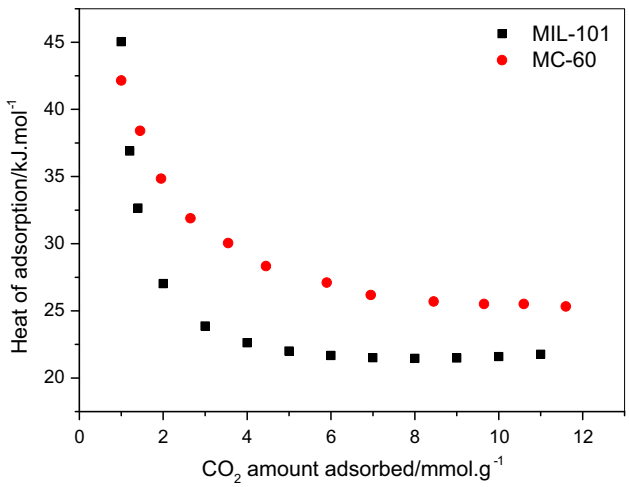


**Fig. 7** $CO_2$ adsorption heat on MIL-101

sites. However, there is a bigger difference in heat between MIL-101 and MC-60 with the increased surface coverage. Moreover, the heat adsorption falling rate for MC-60 sample is lower in comparison with MIL-101, which may be due to a larger number of unsaturated metal sites and higher micropore volume in MC-60 than those in MIL-101. Although the initial adsorption heat is relatively high (about 45 kJ/mol), the binding strengths between unsaturated metal sites and $CO_2$ are still in the regime of physisorption (Wu et al. 2010). Therefore, it is the physical adsorption between MC composite and $CO_2$ molecules that makes $CO_2$ adsorption on MC composite reversible.

In order to verify the reversible $CO_2$ adsorption on MC composite, $CO_2$ adsorption–desorption isotherm on the MC-60 composite was collected at 308 K. As shown in Fig. 10, the desorption isotherm coincides exactly with the adsorption one, indicating $CO_2$ adsorption on the MC composite was completely reversible.

Nevertheless, MIL-101 and MC composites here were prepared and tested in the same way, so the effect on their $CO_2$ adsorption isotherms was similar. Thus, from Fig. 6, we found that the addition of CMK-3 results in a considerable improvement in $CO_2$ adsorption capacity for MC composites when compared to MIL-101. Such improvement could be attributed two reasons. One reason may be the increased number of UMS in MC composites as the interposition of CMK-3 material which could bring out steric hindrance effect and prevent the coordination of unreacted $H_2BDC$ with UMS, resulting in more exposed active sites. Another reason may be the formation of new additional micropores at the interface between the CMK-3 segments and MIL-101 crystals, which was later confirmed by $CO_2$ adsorption studies at 273 K. As shown in Fig. 6, $CO_2$ uptake for MC composites at 1 bar was about 2.67 mmol/g. The value was comparable to $CO_2$ capacities of HKUST-1/graphite oxide and HKUST-1/aminated graphite oxide composites (Kumar et al. 2013; Policicchio et al. 2014).

From a theoretical point of view, the measured values of $CO_2$ capacities on MC composites were compared with the hypothetical ones, which correspond to the values of the physical mixture of MIL-101 and CMK-3. These hypothetical $CO_2$ uptakes for MC composites could be calculated from the percentage of each component in composites and the $CO_2$ capacity of MIL-101 and CMK-3 alone, as listed in the following equation.

$$n_x = n_{MIL-101} \times wt\ \%_{MIL-1101} + n_{CMK-3} \times wt\%_{CMK-3} \quad (1)$$

n presents the hypothetical $CO_2$ uptake of composite x which is MC-30 or MC-60 in our paper, $n_{MIL-101}$ and $n_{CMK-3}$ are the $CO_2$ capacities of MIL-101 and CMK-3 separately, and $wt\%_{MIL-101}$ and $wt\%_{CMK-3}$ represent the weight content of MIL-101 and CMK-3 in composite. The calculated hypothetical $CO_2$ uptakes for MC-30 and MC-60 composites at 298 K and 1 bar are 1.55 and 1.57 mmol/g, respectively. The hypothetical values are much lower than the measured values of MC composites (2.67 mmol/g at 298 K and 1 bar). This reveals the presence of a synergy between the two components. Although the measured $CO_2$ uptakes for MC composites are much close to that of pure CMK-3, this does not affect the conclusion that there is a interplay between MIL-101 and CMK-3 component because the content of carbon phase CMK-3 is very low which leads to the contribution of CMK-3 to $CO_2$ uptakes of composites is negligible.

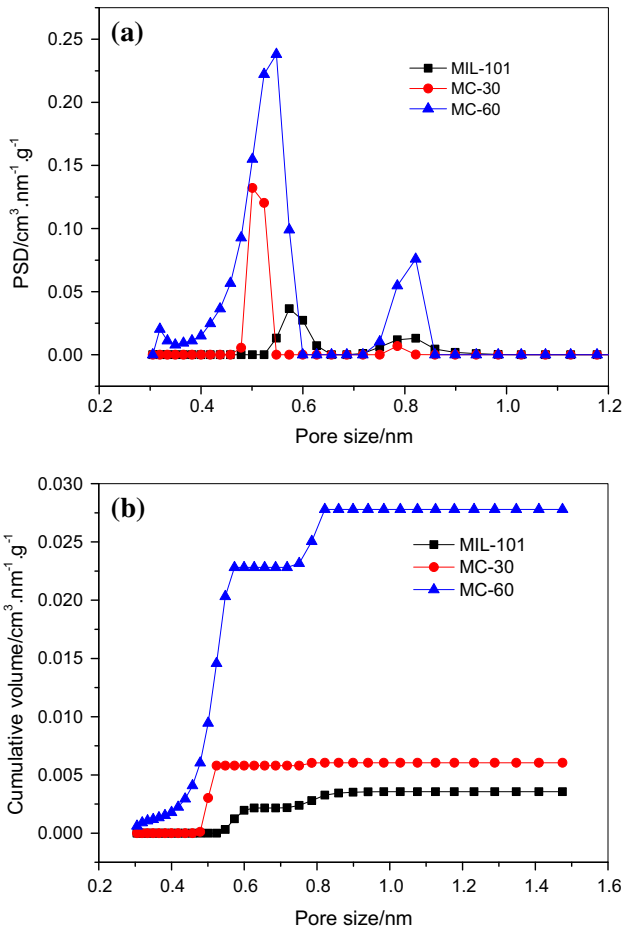


**Fig. 8** PSD curves of MIL-101 and MC composites with DFT method by **a** incremental pore volume and **b** cumulative pore volume

Pore size (below 1 nm) was not obtained from BJH method using nitrogen as an adsorbent from Fig. 5. Thus, $CO_2$ adsorption isotherms at 273 K for MIL-101 and composite materials were collected. On the basis of these $CO_2$ isotherms at 273 K, the PSD curves of MIL-101 and MC composites were calculated using the DFT method and shown in Fig. 8. The PSD data can be divided into two

regimes with pore sizes of 0.3-0.7 nm (I) and 0.7–0.9 nm (II). Both MIL-101 and MC composites show a peak in regime II, which are corresponded to the pore width of super-tetrahedral (ST) building units of MIL-101 (0.86 nm), and an increase in the pore volume in this regime was observed for the composite materials, especially for MC-60. In regime I, there was also a significant increase in the pore volume for composite materials when compared with MIL-101. Besides, a decrease in the pore diameter in regime I was exhibited. Even more important, the composite material, especially for MC-60, shows the formation of additional ultramicropores in the range of 0.3-0.5 nm, which were not present in parent MIL-101. Thus, the $CO_2$-DFT studies clearly suggest the increase in micropore volume, decrease in micropore diameter and formation of additional micropores after CMK-3 incorporation.

As we known, the smaller the pore size, the more favorable to gas adsorption at low pressure because of the strong adsorption potential in small pores. However, we found an interesting result that there is no difference in $CO_2$ uptakes for MC-30 and MC-60 materials, although micropore size is significantly different. Thus, in our opinion, the reason may be attributed to the different amounts of UMS between MC-30 and MC-60. As mentioned above, the incorporation of CMK-3 could result in more exposed UMS in MC composites, but exposed UMS in turn maybe covered by extra carbon when extra CMK-3 material was added in the synthesis of MC-60 composite. On the other hand, crystallinity may be another prime factor influencing $CO_2$ uptakes. As we can see from Fig. 3c, the surface of MC-60 material is very rough and degree of crystallinity is not as good as MC-30, which also can reduce the amounts of UMS. Therefore, we think that the combined effect of both micropores and UMS are responsible for the same $CO_2$ uptake capacities for MC-30 and MC-60 materials.

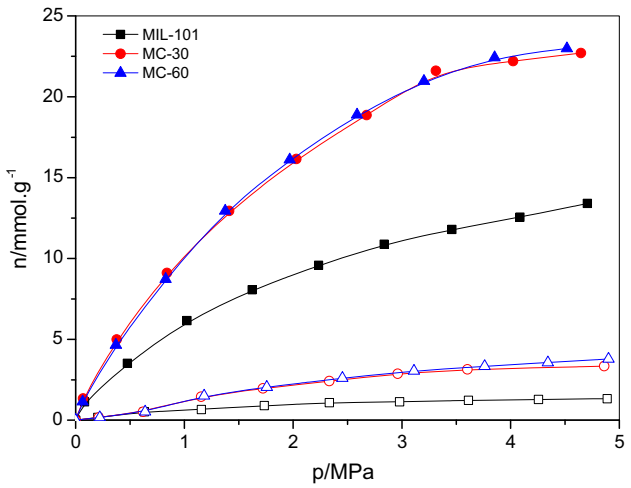


**Fig. 9** $CO_2$ and $N_2$ adsorption isotherms at 298 K

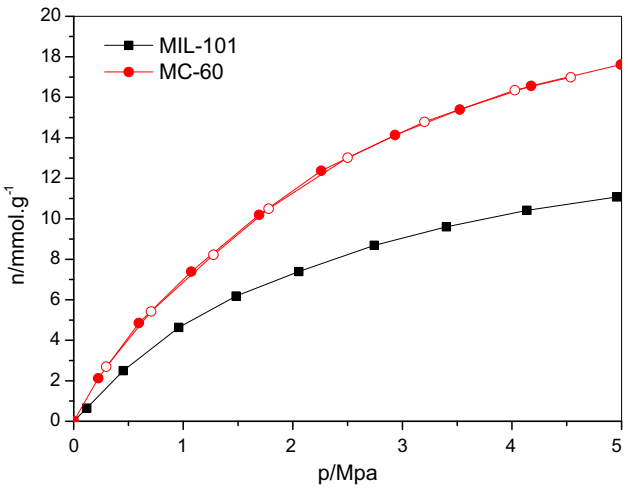


**Fig. 10** $CO_2$ adsorption (solid)-desorption (*open*) isotherms on MIL-101 and MC-60 at 308 K

At last, the high-pressure adsorption isotherms of $CO_2$ and $N_2$ were collected at 298 K up to 5.0 MPa to examine the separation selectivity between $CO_2$ and $N_2$ for MC composites as well as MIL-101, shown in Fig. 8. When CMK-3 was incorporated, $CO_2$ storage capacity of MC composites was enhanced by 77.51 % at 4.5 MPa. However, the selectivity of $CO_2$ over $N_2$ on composites calculated from the ratio of $CO_2$ uptake and $N_2$ uptake under 1 bar was slightly decreased from 9.97 to 6.87 when compared with that on MIL-101 (Figs 9, 10)

## 4 Conclusions

In conclusion, we have successfully synthesized in situ using hydrothermal method and characterized a novel hybrid composite designated MC. This MC composite material exhibits a significant increase in $CO_2$ adsorption capacity at room temperature because of the formation of additional micropores and the activation of unsaturated metal sites by CMK-3 incorporation. These results suggest a new method to improve gas adsorption capacity via the incorporation of other porous materials into MOFs. This approach also presents a new direction for achieving novel MOF hybrid materials.

## References

Arstad, B., Fjellvag, H., Kongshaug, K.O., Swang, O., Blom, R.: Amine functionalized metal organic frameworks (MOFs) as adsorbents for carbon dioxide. Adsorption **14**, 755–762 (2008)

Buso, D., Nairn, K.M., Gimona, M., Hill, A.J., Falcaro, P.: Fast synthesis of MOF-5 microcrystals using sol-gel $SiO_2$ nanoparticles. Chem. Mater. **23**, 929–934 (2011)

Chang, F., Chao, K., Cheng, H., Tan, C.: Adsorption of $CO_2$ onto amine-grafted mesoprous silicas. Sep. Purif. Technol. **70**, 87–95 (2009)

Férey, G., Mellot-Draznieks, C., Serre, C., Millange, F., Dutour, J., Surblé, S., Margiolaki, I.A.: A chromium terephthalate-based solid with unusually large pore volumes and surface area. Science **309**, 2040–2042 (2005)

Furukawa, H., Ko, N., Go, Y.B., Aratani, N., Choi, S.B., Choi, E., Yazaydin, A.O., Snurr, R.Q., Keeffe, M.O., Kim, J., Yaghi, O.M.: Ultra-high porosity in metal-organic frameworks. Science **329**, 424–428 (2010)

Govindasamy, C., Won, J.S., Wha, S.A.: Synthesis of mesoporous materials SBA-15 and CMK-3 from fly ash and their application for $CO_2$ adsorption. J. Porous Mater. **16**, 545–551 (2009)

Guo, B., Chang, L., Xiel, K.: Adsorption of carbon dioxide on activated carbon. J. Nat. Gas Chem. **15**, 223–229 (2006)

Jun, S., Joo, S.H., Ryoo, R., Kruk, M., Jaroniec, M., Liu, Z., Ohsuna, T., Terasaki, O.: Synthesis of new, nanoporous carbon with hexagonally ordered mesostructure. J. Am. Chem. Soc. **122**, 10712–10713 (2000)

Kaye, S.S., Dailly, A., Yaghi, O.M., Long, J.R.: Impact of preparation and handing on the hydrogen storage properties of $Zn_4O$(1,4-benzenedicarboxylate)$_3$ (MOF-5). J. Am. Chem. Soc. **129**, 14176–14177 (2007)

Krungleviciute, V., Lask, K., Heroux, L., Migone, D., Lee, J.Y., Skoulidas, A.: Argon adsorption on $Cu_3$(benzene-1,3,5-tricarboxylate)$_2$($H_2O$)$_3$ metal-organic. Langmuir **23**, 3106–3109 (2007)

Kumar, R., Jayaramule, K., Maji, T.K., Rao, C.N.R.: Hybrid nanocomposites of ZIF-8 with grapheme oxide exhibiting tunable morphology, significant $CO_2$ uptake and other novel properties. Chem. Commun. **49**, 4947–4949 (2013)

Li, L., Wen, X., Fu, X., Wang, F., Zhao, N., Xiao, F.K., Wei, W., Sun, Y.H.: $MgO/Al_2O_3$ sorbent for $CO_2$ capture. Energy Fuels **24**, 5773–5780 (2010)

Li, Y., Sun, N.N., Li, L., Zhao, N., Xiao, F.K., Wei, W., Sun, Y.H., Huang, W.: Grafting of amines on ethanol-extracted SBA-15 for $CO_2$ adsorption. Materials **6**, 981–999 (2013)

Liewellyn, P.L., Bourrelly, S., Serre, C., Vimont, A., Daturi, M., Iiamon, L.: High uptakes of $CO_2$ and $CH_4$ in mesoporous metal-orfanic frameworks MIL-100 and MIL-101. Langmuir **24**, 7245–7250 (2008)

Liu, Y.Y., Zeng, J.L., Zhang, J., Xu, F., Sun, L.X.: Improved hydrogen strorage in the modified metal-organic frameworks by hydrogen spillover effect. Int. J. Hydrogen Energy **32**, 4005–4010 (2007)

Liu, J., Wang, Y., Benin, A.I., Jakubczak, P., Willis, R.R., Levan, M.D.: $CO_2/H_2O$ adsorption equilibrium and rates on metal-organic frameworks: HKUST-1 and Ni/DOBDC. Langmuir **26**, 14301–14307 (2010)

Liu, J., Thallapally, P.K., McGrail, B.P., Brown, D.R., Liu, J.: Process in adsorption-based $CO_2$ capture by metal-organic frameworks. Chem. Soc. Rev. **41**, 2308–2322 (2012)

Maksimchuk, N.V., Timofeeva, M.N., Melgunov, M.S., Shmakov, A.N., Chesalov, Y.A., Dybtsev, D.N., Fedin, V.P., Kholdeeva, O.A.: Heterogeneous selective oxidation catalysts based on coordination polymer MIL-101 and transition metal-substituted polyoxometalates. J. Catal. **257**, 315–323 (2008)

Martacaltzi, C.S., Lemonidou, A.A.: Development of new CaO based sorbent materials for $CO_2$ removal at high temperature. Microporous Mesoporous Mater. **110**, 119–127 (2008)

Millwar, A.R., Yaghi, O.M.: Metal-organic frameworks with exceptionally high capacity for storage of carbon dioxide at room temperature. J. Am. Chem. Soc. **127**, 17998–17999 (2005)

Miyamoto, M., Fujiokax, Y., Yogo, K.: Pure silica CHA type zeolite for $CO_2$ separation using pressure swing adsorption at high pressure. J. Mater. Chem. **22**, 20186–20189 (2012)

Pachfule, P., Balan, B.K., Kurungot, S., Banerjee, R.: One-dimensional confinement of a nanosized metal-organic framework in carbon nanofibers for improved gas adsorption. Chem. Comm. **48**, 2009–2011 (2012)

Petit, C., Bandosz, T.J.: MOF-graphite oxide nanocomposites: surface characteriazation and ecaluation as adsorbents of ammonia. J. Mater. Chem. **19**, 6521–6528 (2009a)

Petit, C., Bandosz, T.J.: MOF-graphite oxide composites: combing the uniqueness of grapheme layers and metal-organic frameworks. Adv. Mater. **21**, 4753–4757 (2009b)

Petit, C., Bandosz, T.J.: Enhanced adsorption of ammonia on metal-organic framework/graphite oxide composites: analysis of surface interactions. Adv. Funct. Mater. **20**, 111–118 (2010)

Petit, C., Mendoza, B., Bandoza, T.: Reactive adsorption of ammonia on Cu-based MOF/grapheme composites. Langmuir **26**, 15302–15309 (2010)

Petit, C., Burress, J., Bandosz, T.J.: The synthesis and characterization of copper-based metal-organic framework/graphite oxide composites. Carbon **49**, 563–572 (2011)

Policicchio, A., Zhao, Y.X., Zhong, Q., Agostino, R.G., Bandosz, T.J.: Cu-BTC/aminated graphite oxide composites as high-efficiency $CO_2$ capture media. ACS Appl. Mater. Interfaces **6**, 101–108 (2014)

Prasanth, K.P., Rallapalli, P., Raj, M.C., Bajaj, H.C., Jasra, R.V.: Enhanced hydrogen sorption in single walled carbon nanotube incorporated MIL-101 composite metal-organic framework. Int. J. Hydrogen Energy **36**, 7594–7601 (2011)

Rallapalli, P.B.S., Raj, M.C., Patil, D.V., Prasanth, P.K., Somani, R.S., Bajaj, H.C.: Activated carbon@MIL-101(Cr): a potential metal-organic framework composite material for hydrogen strorage. Int. J. Energy Res. **37**, 746–753 (2013)

Shao, W., Zhang, L.Z., Li, L.X., Lee, R.L.: Adsorption of $CO_2$ and $N_2$ on synthesized NaY zeolite at high temperatures. Adsorption **15**, 497–505 (2009)

Suddik, A.C., Cote, A.P., Wong-Foy, A.G., O'Keeffe, M., Yaghi, O.M.: A metal-organic framework with a hierarchical system of pores and tetrahedral building blocks. Angew. Chem. Int. Ed. **45**, 2528–2533 (2006)

Sun, Y., Liu, X.W., Su, W., Zhou, Y.P., Zhou, L.: Studies on ordered mesoporous materials for potential environmnental and clean energy applications. Appl. Surf. Sci. **253**, 5650–5655 (2007)

Wong, S., Bioletti, R.: Carbon dioxide separation technologies. Carbon & Energy Management, Alberta Research Council, Edmonton, Alberta, Canada (2002)

Wu, H., Simmons, J.M., Srinivas, G., Zhou, W., Yildirim, T.: Adsorption sites and binding nature of CO2 in prototypical metal-organic frameworks: a combined neutron diffraction and first-principles study. J. Phys. Chem. Lett. **1**, 1946–1951 (2010)

Wu, C.M., Rathi, M., Ahrenkiel, S.P., Koodali, R.T., Wang, Z.Q.: Facile synthesis of MOF-5 confined in SBA-15 hybrid material with enhanced hydrostability. Chem. Comm. **49**, 1223–1225 (2013)

Yang, S.J., Choi, J.Y., Chae, H.K., Cho, J.H., Nahm, K.S., Park, C.R.: Preparation and enhanced hydrostability and hydrogen storage capacity of CNT@MOF-5 hybrid composite. Chem. Mater. **21**, 1893–1897 (2009)

Yang, H., Gong, M., Chen, Y.: Preparation of activated carbons and their adsorption properties for greenhouse gases: $CH_4$ and CO2. J. Nat. Gas Chem. **20**, 460–464 (2011)

Yazaydin, A.O., Snurr, R.Q., Park, T.H., Koh, K., Liu, J., Levan, M.D., Benin, A.I., Jakubazak, P., Lanuza, M., Galloway, D.B., Low, J.J., Willis, R.R.: Screening of metal-organic frameworks for carbon dioxide capture from flue gas using a combined

experimental and modeling approach. J. Am. Chem. Soc. **131**, 18198–18199 (2009)

Zhang, Z.Z., Ruan, H.Z., Zhou, Y.P., Su, W., Sun, Y., Zhou, L.: A research note on the adsorption of $CO_2$ and $N_2$. Chin. J. Chem. Eng. **19**, 733–737 (2011)

Zhang, Z.Z., Tang, J.D., Sun, Y., Su, W.: Water effect on amine-modification of adsorbents for separation of $CO_2/N_2$. Trans. Tianjin Univ. **19**, 313–318 (2013)

Zhao, D.Y., Feng, J.L., Huo, Q.S., Melosh, N., Fredrickson, G.H., Chmelka, B.F., Stucky, G.D.: Triblock copolymer synthesis of mesoporous silica with periodic 50 to 300 Angstrom pores. Science **279**, 548–552 (1998)

Zhao, Y.X., Seredych, M., Zhong, Q., Bandosz, T.J.: Superior performance of copper based MOF and aminated graphite oxide composites as $CO_2$ adsorbents at room temperature. ACS Appl. Mater. Interfaces **5**, 4951–4959 (2013)

Zhao, Y.X., Seredych, M., Jagiello, J., Zhong, Q., Bandosz, T.J.: Insight into the mechanism of $CO_2$ adsorption on Cu-BTC and its composites with graphite oxide or aminated graphite oxide. Chem. Eng. J. **239**, 399–407 (2014)